Chapter 6

The Study of Cu^{II} Phenolate Redox Chemistry

The reactions of phenol with copper are numerous and versatile, including biomimetic ring-oxygenations and many different oxidative phenol coupling reactions. We report here an unprecedented redox conversion between Cu^{II} and different phenolate compounds. Controlled oxidation of a Cu^{I} complex coordinated to phenol leads to formation of a purple Cu^{II} phenolate complex that was analyzed by X-ray crystallography, EPR and cyclic voltammetry. This mononuclear complex was found to convert intermolecularly to a Cu^{I} species and a phenol-derived product that can be either a diaryl peroxide or an aromatic ether. UV-vis and NMR spectroscopy confirmed formation of a diamagnetic Cu^{I} species and the Raman spectrum showed the presence of a new aryl-O bond. Interestingly, this new redox chemistry is very similar to the Cu^{II} μ-thiolate/Cu^{I} disulfide redox chemistry.

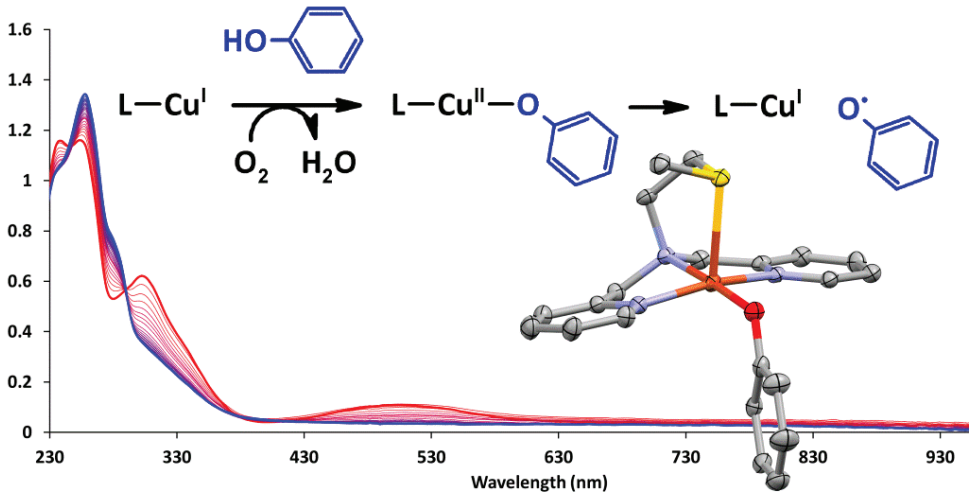

This chapter will be published: E. C. M. Ording-Wenker, M. J. B. Moester, M. A. Siegler, E. Bouwman, *manuscript in preparation*.

6.1 Introduction

Copper-oxygen chemistry is a research field of great interest because of the essential role it plays in many biological processes such as oxygen transfer, hydrogen peroxide generation, methane oxidation and aromatic ring oxygenation.[1, 2] The aromatic ring oxygenation of phenols to catechols and further to *ortho*-quinones has received a lot of attention, owing to its relevance to the tyrosinase and catechol oxidase activity (section 1.2.3; Chapter 7). Furthermore, a large range of substituted phenol substrates is available that allows tweaking of the reaction for mechanistic research.[2-6] Apart from the biomimetic phenol oxygenations, research has been focused on oxidative phenol coupling to form diphenols, diphenoquinones, cyclized products and polymers.[7] Despite the fact that a tremendous amount of research on copper-phenol chemistry has been reported, in this chapter we report unprecedented reactivity in which Cu^{II} and phenolate (PhO^-) form Cu^{I} and a phenolate radical ($PhO^{\bullet}$) that reacts further to an unknown product, as schematically shown in Figure 6.1. This chemistry exhibits similarities to the Cu^{II} μ-thiolate and Cu^{I} disulfide redox chemistry discussed in previous chapters.

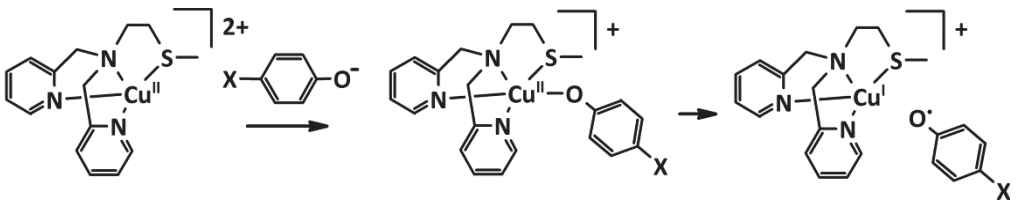

Figure 6.1: Schematic representation of the reaction between $[Cu^{II}(\mathbf{L^1SCH_3})]^{2+}$ and a *para*-substituted phenolate resulting in Cu^{I} and phenolate-peroxide. X = H, halogen, OMe or alkyl.

6.2 Results and Discussion

6.2.1 Synthesis and Analysis of Cu^{II} Complexes

The ligand $\mathbf{L^1SCH_3}$ (Figure 6.1) has been used in our investigations, because it is similar to the ligand $\mathbf{L^1SSL^1}$ that forms Cu^{II} μ-thiolate complexes with Cu^{I} salts (Chapter 2). The presence of the thioether moiety prohibits μ-thiolate formation as the thiolate group has been reported to react with the phenolate moiety.[8] The ligand $\mathbf{L^1SCH_3}$ was synthesized by reductive amination of 2-(methylthio)ethylamine, avoiding the use of toxic 2-chloroethyl methyl sulfide,[9] and increasing the yield from 53% to 99%. The orange/yellow oil of $\mathbf{L^1SCH_3}$ slowly turns dark brown when kept for longer periods of time (weeks). When a flask containing a mixture of equimolar

amounts of $[Cu^{I}(CH_3CN)_4]^+$, **L^1SCH_3** and PhOH in CH_3CN is opened to air an intense dark purple solution is obtained (see Figure 6.2).

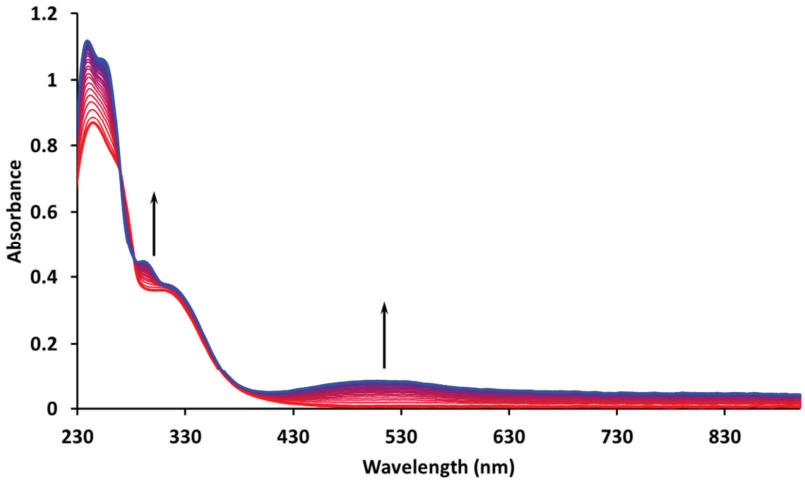

Figure 6.2: UV-vis spectroscopic changes observed for the oxidation of a mixture of $[Cu^{I}(\mathbf{L^1SCH_3})](SbF_6)$ and PhOH by air in CH_3CN at 1.0 mM [Cu] concentration. Spectra were measured over a period of 2 hrs with a transmission dipprobe set at a path length of 1.2 mm.

The UV-vis spectrum shows absorption bands at 238, 255, 293, 320, 510 and 840 nm. The absorption bands at 238, 255, 293 and 320 nm likely arise from LMCT transitions, while the absorptions at 510 and 840 nm can be assigned to Cu^{II} d-d transitions. The bands at 310 and 510 nm are similar to the absorption bands that have been assigned to a Cu^{II}_2 μ-η^2:η^2-peroxide species (~360 nm and 510 nm).[10] To investigate whether a Cu-peroxide species is indeed formed the Raman spectra of copper compounds with a range of different *para*-substituted phenols were measured. Although some of these compounds indeed show a Raman signal close to 740 cm^{-1}, as expected for a Cu_2-peroxide species, for most complexes we observe that the position of this signal shifted depending on the substituent on the *para*-position of the phenyl group. These signals are observed in the range between 580 and 780 cm^{-1} and can possibly be assigned to the C-H out of plane deformations and ring deformations of the phenyl ring (Appendix V, Figure AV.1).[11]

Several reports of purple copper compounds have ascribed the UV-Vis spectra to the presence of Cu^{III}.[12-15] To validate this option, an X-band EPR spectrum of the purple complex in CH_3CN at room temperature was measured. The EPR spectrum shows a

mononuclear isotropic signal with $g_i = 2.10$ and copper hyperfine splitting of 52 Gauss (Appendix V, Figure AV.2), in agreement with the presence of Cu^{II} instead of Cu^{III}. Initially the purple Cu^{II} phenolate complex $[Cu^{II}(\mathbf{L^1SCH_3})(OPh\text{-}X)]^+$ was obtained from a Cu^{I} complex in the presence of phenol and dioxygen, following equation (1). However, the same compound can also be synthesized starting from a Cu^{II} complex and a phenolate salt under oxygen-free conditions, according to equation (2).

$$4\,[Cu^{I}(\mathbf{L^1SCH_3})]^+ + 4\,X\text{-}PhOH + O_2 \rightarrow 4\,[Cu^{II}(\mathbf{L^1SCH_3})(OPh\text{-}X)]^+ + 2\,H_2O \quad (1)$$

$$[Cu^{II}(\mathbf{L^1SCH_3})]^{2+} + X\text{-}PhO^- \rightarrow [Cu^{II}(\mathbf{L^1SCH_3})(OPh\text{-}X)]^+ \quad (2)$$

When the purple complex was prepared in CH_2Cl_2 and the solution was cooled to –84 °C, dark-brown crystals formed. X-ray structure determination showed that the obtained crystals consisted of $[Cu^{II}(\mathbf{L^1SCH_3})(OPh)](SbF_6) \cdot PhOH \cdot 0.38\ CH_2Cl_2$. Attempts to grow crystals at –20 °C of a solution containing *p*-cresol (Me-PhOH), led to formation of single crystals, that by X-ray diffraction were shown to be composed of $[Cu^{II}(\mathbf{L^1SCH_3}^*)(OPh\text{-}Me)](PF_6) \cdot Me\text{-}PhOH \cdot 1.75\ CH_2Cl_2$, in which $\mathbf{L^1SCH_3}^*$ is a degraded ligand. Further analysis of this compound could not be performed, due to its accidental formation in low yield and poor reproducibility. However, as we believe that the formation of this compound is typical for the degradation of this type of complexes, we judged that it is worthwhile to discuss the structure.

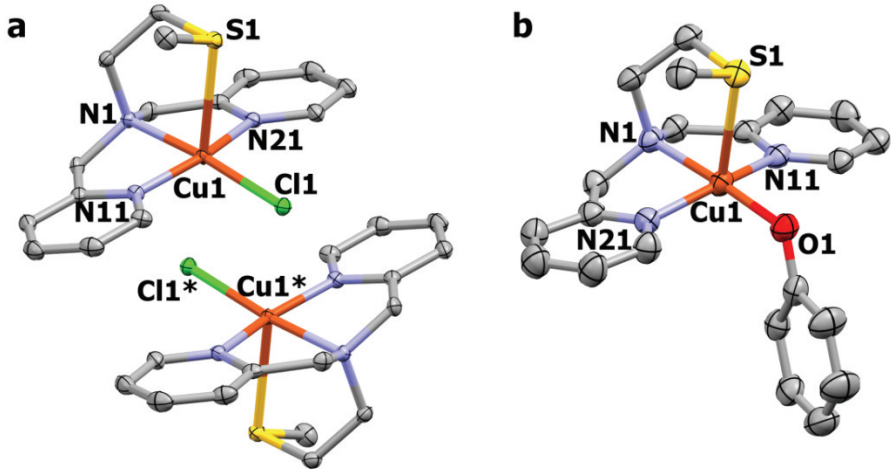

Figure 6.3: Displacement ellipsoid plots (50% probability level) of (a) two cationic complexes of $[Cu^{II}(\mathbf{L^1SCH_3})(Cl)](BF_4)$ and (b) one cationic molecule of $[Cu^{II}(\mathbf{L^1SCH_3})(OPh)](SbF_6) \cdot PhOH \cdot 0.38\ CH_2Cl_2$. The non-coordinating counterions, hydrogen atoms and co-crystallized solvents are omitted for clarity. Symmetry operation * = [1–x, 2–y, 1–z].

For comparison the compound [Cu^{II}(**L^1SCH_3**)(Cl)](BF_4) was synthesized from a mixture containing [$Cu^{II}(H_2O)_6$](BF_4)$_2$, $CuCl_2 \cdot 2\ H_2O$ and **L^1SCH_3** and its structure was determined by X-ray crystallography. Displacement ellipsoid plots of the cationic complexes in [Cu^{II}(**L^1SCH_3**)(Cl)](BF_4), [Cu^{II}(**L^1SCH_3**)(OPh)](SbF_6) and [Cu^{II}(**L^1SCH_3***)(OPh-Me)](PF_6) are shown in Figure 6.3 and Figure 6.4. Crystallographic data and selected bond distances and angles are given in Table 6.1 and Table 6.2. [Cu^{II}(**L^1SCH_3**)(Cl)](BF_4) crystallizes in the triclinic space group *P*-1. The copper ion is in an elongated octahedral coordination geometry with N_3SCl_2 environment, forming a dimer through a weak interaction with a chloride ion (3.1018(4) Å) from a neighboring molecule. The Cu-Cu* distance is 3.8192(3) Å.

Table 6.1: Crystallographic and structure refinement data for complexes [Cu^{II}(**L^1SCH_3**)(Cl)](BF_4), [Cu^{II}(**L^1SCH_3**)(OPh)](SbF_6) and [Cu^{II}(**L^1SCH_3***)(OPh-Me)](PF_6).

	[Cu^{II}(**L^1SCH_3**)(Cl)](BF_4)	[Cu^{II}(**L^1SCH_3**)(OPh)](SbF_6)	[Cu^{II}(**L^1SCH_3***)(OPh-Me)](PF_6)
empirical formula	$[C_{15}H_{19}ClCuN_3S](BF_4)$	$[C_{21}H_{24}CuN_3OS](SbF_6) \cdot C_6H_5OH \cdot 0.38\ CH_2Cl_2$	$[C_{28}H_{29}CuN_4O_2S](PF_6) \cdot C_7H_7OH \cdot 1.75\ CH_2Cl_2$
formula weight	459.19	1583.47	950.51
crystal system	triclinic	monoclinic	triclinic
space group	*P*-1	*C*2/c	*P*-1
a, Å	7.45273(18)	28.9170(8)	11.5835(3)
b, Å	11.2448(3)	22.0004(5)	14.5137(4)
c, Å	12.3634(3)	10.6154(2)	14.5908(4)
α, deg	65.993(3)	90	66.815(3)
β, deg	74.934(2)	90.013(2)	74.239(2)
γ, deg	88.273(2)	90	68.573(3)
V, Å^3	910.58(4)	6753.4(3)	2075.50(11)
Z	2	4	2
D_{calc}, g·cm^3	1.675	1.557	1.518
T, K	110(2)	110(2)	110(2)
crystal size, mm	$0.36 \times 0.28 \times 0.22$	$0.36 \times 0.08 \times 0.07$	$0.64 \times 0.31 \times 0.08$
μ, mm^{-1}	1.504	8.792	4.229
no. of reflns measd	28025	20658	25599
no. of unique reflns	4179	6624	8055
no. of reflns obsd.	3994 [$I > 2\sigma(I)$]	6263 [$I > 2\sigma(I)$]	7606 [$I > 2\sigma(I)$]
no. of parameters	282	502	616
R_1 / wR_2 [$I > 2\sigma(I)$]	0.0187/0.0486	0.0451/0.1256	0.0671/0.1764
R_1 / wR_2 [all refl.]	0.0197/0.0491	0.0479/0.1281	0.0696/0.1783
goodness of fit	1.043	1.077	1.129
$\Delta\rho$, e·Å^{-3}	–0.30/0.36	–0.86/1.01	–0.77/1.10

Table 6.2: Selected bond distances (Å) and bond angles (°) complexes [Cu^{II}(**L^1SCH_3**)(Cl)](BF_4), [Cu^{II}(**L^1SCH_3**)(OPh)](SbF_6) and [Cu^{II}(**L^1SCH_3***)(OPh-Me)](PF_6).

	[Cu^{II}(**L^1SCH_3**)(Cl)](BF_4)	[Cu^{II}(**L^1SCH_3**)(OPh)](SbF_6)	[Cu^{II}(**L^1SCH_3***)(OPh-Me)](PF_6)
Cu1 - Cu1*	3.8192(3)		
Cu1 - S1	2.7152(4)	2.6270(15)	2.5796(11)
Cu1 - N1	2.0558(10)	2.063(4)	2.071(3)
Cu1 - N11	1.9782(11)	1.985(4)	1.993(4)
Cu1 - N21	1.9845(11)	1.984(4)	1.980(3)
Cu1 - Cl1/O1	2.2588(3)	1.929(4)	3.249(3)
Cu1 - Cl1*/F6/O2	3.1018(4)	3.398(4)	1.907(3)
S1 - Cu1 - N1	85.93(3)	87.47(12)	86.17(9)
S1 - Cu1 - N11	101.67(3)	91.62(12)	106.77(10)
S1 - Cu1 - N21	84.59(3)	103.05(13)	97.55(9)
S1 - Cu1 - Cl1/O1/O2	100.430(11)	95.17(12)	93.62(9)
N1 - Cu1 - N11	82.43(4)	83.77(17)	82.29(14)
N1 - Cu1 - N21	83.42(4)	82.59(18)	83.71(13)
N1 - Cu1 - Cl1/O1/O2	173.64(3)	177.09(17)	177.63(13)
N11 - Cu1 - N21	164.06(4)	159.44(18)	150.92(14)

Symmetry operation * = [1–x, 2–y, 1–z]

[Cu^{II}(**L^1SCH_3**)(OPh)](SbF_6) crystallizes in the monoclinic space group *C*2/c. The SbF_6^- counterion and the phenol molecule are both found to be disordered over two orientations; the occupancy factors of the major components of the disorder refines to 0.938(3) and 0.560(11), respectively. Furthermore, the crystal lattice contains CH_2Cl_2 molecules that are located at sites of twofold axial symmetry.[16] In contrast to [Cu^{II}(**L^1SCH_3**)(Cl)](BF_4), [Cu^{II}(**L^1SCH_3**)(OPh)](SbF_6) does not form a dimeric species. The copper ion is in a square-pyramidal geometry (τ = 0.29)[17] and seems to have a weak interaction with the SbF_6^- counterion (Cu – F6 = 3.398(4) Å). The phenol lattice molecule forms a hydrogen bond with the coordinated phenolate molecule at a PhO…H-OPh distance of 1.78 Å. [Cu^{II}(**L^1SCH_3***)(OPh-Me)](PF_6) crystallizes in the triclinic space group *P*-1. The coordinated *p*-cresolate is found to be disordered over two orientations; the occupancy factor of the major component of the disorder refines to 0.722(17). The crystal lattice contains two partially occupied CH_2Cl_2 molecules per asymmetric unit.[18] The copper ion in [Cu^{II}(**L^1SCH_3***)(OPh-Me)](PF_6) has a coordination geometry that is very similar to that in [Cu^{II}(**L^1SCH_3**)(OPh)](SbF_6). The square-pyramidal geometry is more distorted (τ = 0.46) due to the strain in the backbone of the ligand, caused by the oxidative degradation. The degradation of the ligand resulted in formation of a new five-membered ring at the benzylic positions of the pyridyl groups. The five-membered ring seems to have been formed from the

coordinating ligand and an (at the benzylic position) oxidized pyridyl group of another ligand. It has been reported that these benzylic positions can be reactive, which might also explain the rapid degradation of the free ligand **L^{1}SCH$_3$**.[19-22]

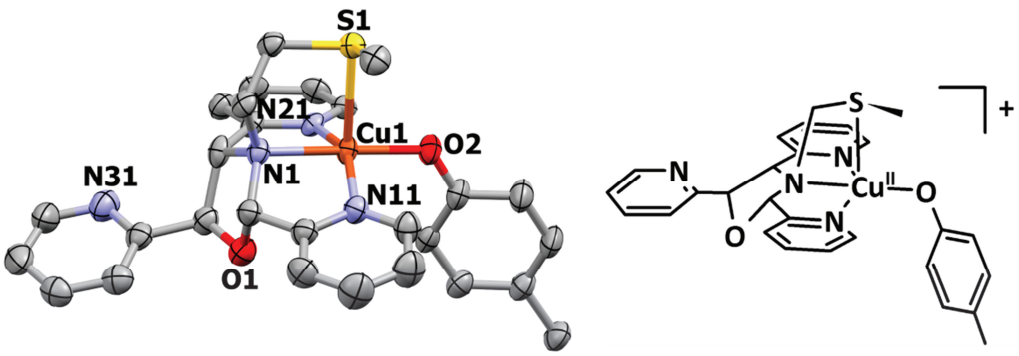

Figure 6.4: Schematic drawing and displacement ellipsoid plot (50% probability level) of the cationic part of [Cu^{II}(**L^{1}SCH$_3$***)(OPh-Me)](PF$_6$) · Me-PhOH · 1.75 CH_2Cl_2. The non-coordinating counterion, hydrogen atoms and lattice molecules have been omitted for clarity.

Cyclic voltammograms were recorded of [Cu^{II}(**L^{1}SCH$_3$**)(OPh-Me)]$^+$ in CH_3CN (see Figure 6.5); this solution is stable for several days at room temperature. An equimolar mixture of **L^{1}SCH$_3$** with Cu^{II}(OTf)$_2$ in CH_3CN shows a reversible redox event corresponding to the Cu^{II}/Cu^{I} redox couple at a half-wave potential of $E_{1/2}$ = +0.19 V vs Ag/AgCl with a peak-to-peak separation of 81 mV. Me-PhO$^-$ (as the potassium salt) in CH_3CN shows two irreversible oxidation events at +0.03 V and +0.31 V vs Ag/AgCl. The oxidation event at +0.03 V likely corresponds to the formation of the cresolate radical: Me-PhO$^-$ → Me-PhO$^\bullet$. The voltammogram of the purple Cu^{II} cresolate compound shows three quasi-reversible and one irreversible redox-event. The irreversible oxidation wave at E_{pa} = 0.81 V and the quasi-reversible event at $E_{1/2}$ = +1.02 V are very similar to the waves observed for M-PhO$^-$, albeit considerably shifted. The quasi-reversible redox couple at $E_{1/2}$ = –0.34 V can be assigned to the Cu^{II}/Cu^{I} couple of the copper cresolate complex; the more negative $E_{1/2}$ value is in agreement with stabilization of the Cu^{II} oxidation state by the coordinating *p*-cresolate anion. The redox event at $E_{1/2}$ = +0.17 V is likely to originate from the Cu^{II}/Cu^{I} redox couple of the complex without a coordinating cresolate group; its intensity is strongly dependent on scan rate (Appendix V, Figure AV.3).

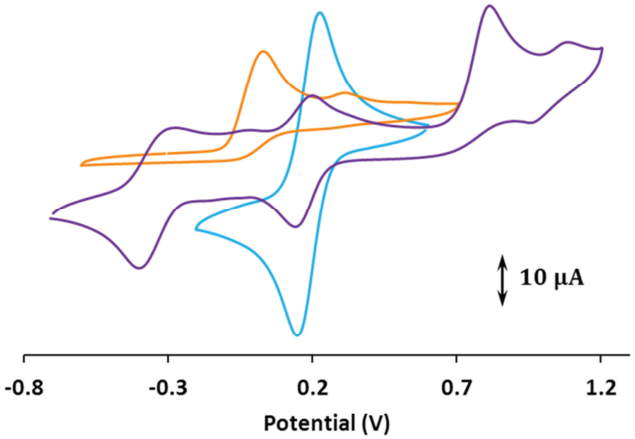

Figure 6.5: Cyclic voltammograms of Me-PhOK (orange), $Cu^{II}(OTf)_2$ + $\mathbf{L^1SCH_3}$ (blue) and $[Cu^{II}(\mathbf{L^1SCH_3})(OPh\text{-}Me)](OTf)$ (purple) in CH_3CN at 2.0 mM [Cu] concentration measured with a scan rate of 100 mV/s. Potentials are given vs Ag/AgCl.

6.2.2 Cu^{II} Phenolate Conversion

Over time the color of a Cu^{II} phenolate solution kept under an argon atmosphere changes from purple to yellow. The change from purple to yellow was monitored with UV-vis spectroscopy for a solution containing $[Cu^{II}(\mathbf{L^1SCH_3})(OPh\text{-}F)](OTf)$ (Figure 6.6). The rate of this conversion depends on the *para*-substituent at the phenol ring. The stability of the purple complexes decreases approximately in the order of X = OMe > tert-butyl ~ iso-propyl ~ CH_3 > H > Cl ~ Br ~ I > F > CF_3. The presence of electron-donating substituents prolongs the lifetime of the purple species, while electron-withdrawing groups result in faster conversion towards the yellow product. In methanol, the purple compound is stable for a short time, but the use of the non-protic solvent CH_3CN increases the lifetime of the purple complex significantly. At low complex concentrations the conversion to the yellow product is much slower (> 50 hrs at 1.0 mM [Cu], Figure 6.6a) than at higher concentrations (~15 min at 10 mM [Cu], Figure 6.6b), indicating that an intermolecular process takes place. The LMCT at 300 nm and the Cu^{II} d-d transitions at 500 and 840 nm disappear, indicating that a Cu^{I} species is formed, and new absorption bands at 257 and 280 nm appear. The formation of Cu^{I} is confirmed by the diamagnetic ^1H NMR spectrum, which resembles that of a 1:1 mixture of $[Cu^{I}(\mathbf{L^1SCH_3})](OTf)$ and F-PhOH (Figure 6.7). The spectrum showed that already some degradation of the ligand had occurred, which is potentially similar as witnessed in $[Cu^{II}(\mathbf{L^1SCH_3}^*)(OPh\text{-}Me)](PF_6)$ (Figure 6.4).

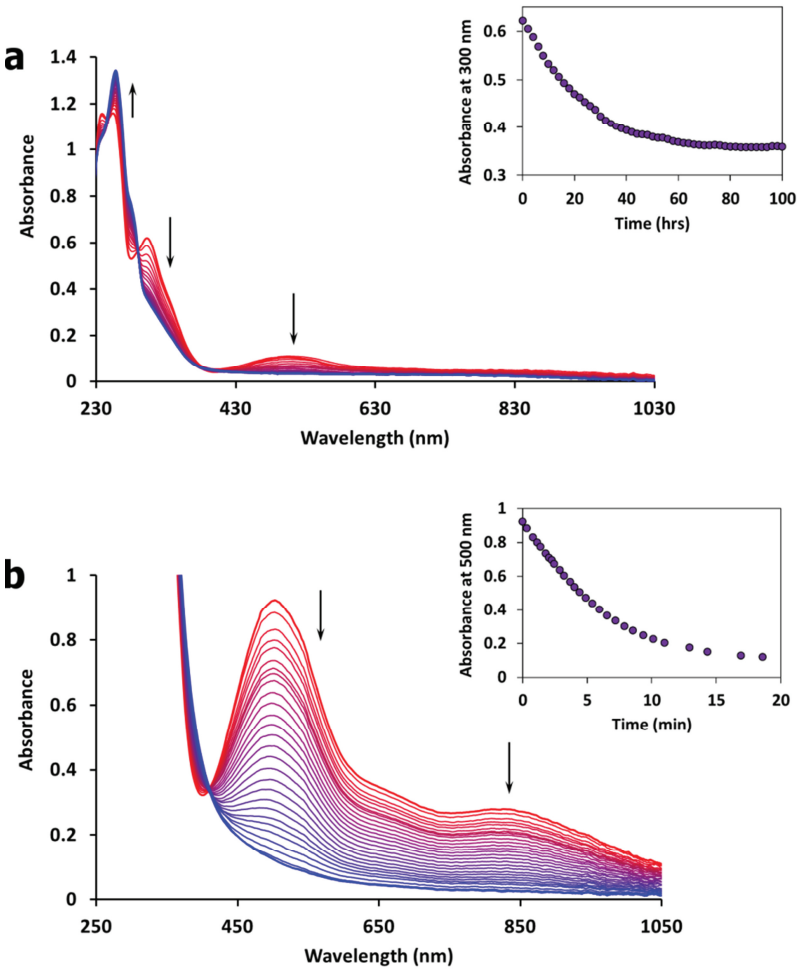

Figure 6.6: UV-vis spectroscopic changes of the conversion of the purple compound [Cu^{II}(**L^1SCH_3**)(OPh-F)](OTf) in CH_3CN to a yellow-colored solution (a) at 1.0 mM [Cu] concentration for 100 hrs and (b) at 10 mM [Cu] concentration for 19 min. Spectra were recorded with a transmission dipprobe set at a path length of 1.2 mm. The inset and the arrows indicate the development of the spectra over time.

The fact that Cu^{II} has reduced to Cu^{I} means that an electron has transferred from PhO^- to copper creating a $PhO^\bullet$ radical that will react further. The concentration-dependence of the conversion indicates that an intermolecular reaction takes place, which could mean that the phenolate radicals react with each other. However, o*rtho*-substitution or oxidative polymerization of the phenol radicals is not likely as this would result in different (asymmetric) NMR spectra. Alternatively, the radical might react with **L^1SCH_3** or the solvent or it may pick up an $H^\bullet$ to reform the phenol

compound. Another option is that two of these phenolate radicals react together to form the peroxide PhO-OPh.

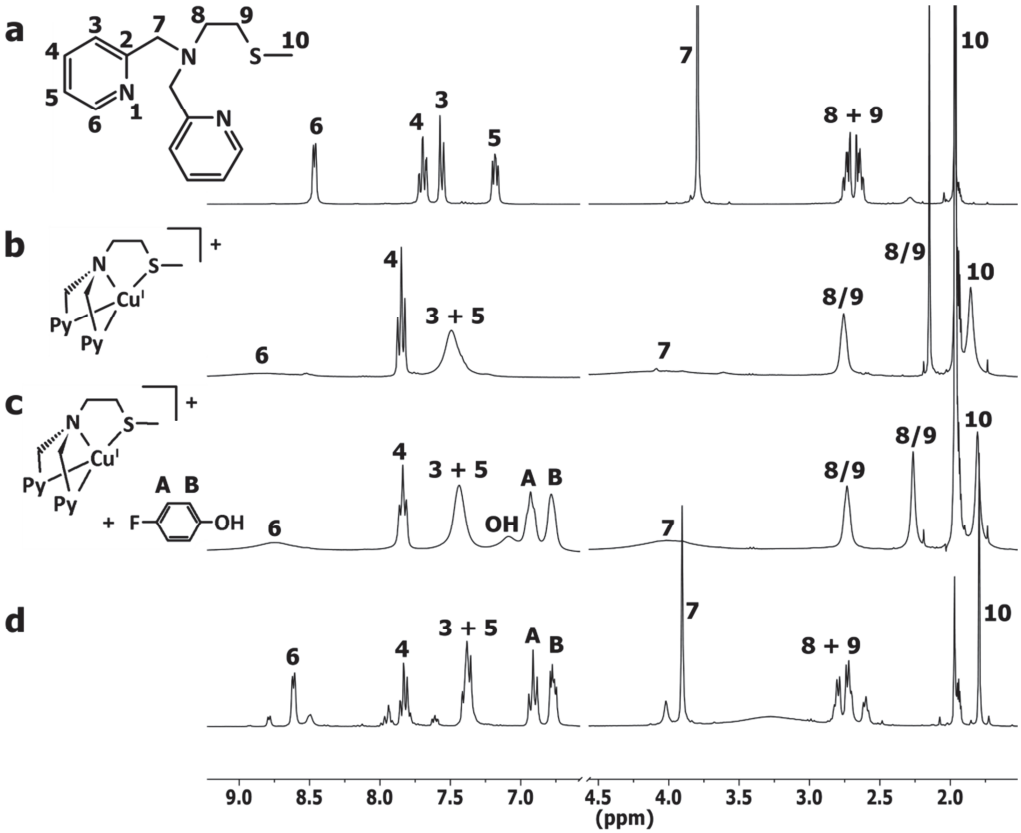

Figure 6.7: ^{1}H NMR spectra of (a) $\mathbf{L^{1}SCH_{3}}$, (b) [Cu^{I}($\mathbf{L^{1}SCH_{3}}$)](OTf), (c) a mixture of [Cu^{I}($\mathbf{L^{1}SCH_{3}}$)](OTf) and F-PhOH and (d) the yellow solution obtained after reaction of [Cu^{II}($\mathbf{L^{1}SCH_{3}}$)](OTf)$_2$ with F-PhO$^-$ in CD_3CN at RT.

To check for the formation of a new bond, Raman spectroscopy was used. The Raman spectra of the purple complex [Cu^{II}($\mathbf{L^{1}SCH_{3}}$)(OPh-F)](OTf) and its converted yellow species are shown in Figure 6.8. The spectra are virtually the same except for an extra Raman signal at 1033 cm^{-1} in the spectrum of the yellow solution. This signal is blue-shifted compared to the O-O stretch vibrations reported for dialkyl-peroxides (~850-900 cm^{-1}).[23] However, this vibration could be assigned to the C-O stretch vibration of an aryl peroxide, which is reported to be located around 1000 cm^{-1}, whereas the C-O stretch vibration for *p*-substituted phenols is located between 1200-1300 cm^{-1}.[11, 24] There are theoretical studies that have shown that the formation of a diaryl peroxide

is unfavorable.[25, 26] Conversely, there are also theoretical studies[27, 28] and some experimental reports in which the formation of diaryl peroxides is thought to occur.[29-36] Alternatively, the signal at 1033 cm^{-1} can be assigned to the C-O stretch vibration of an aromatic ether (1010-1050 cm^{-1})[37] which could form if the $PhO^{\bullet}$ species reacts with the solvent or the ligand. In both cases however, the appearance of this C-O signal indicates the formation of a new species other than phenol.

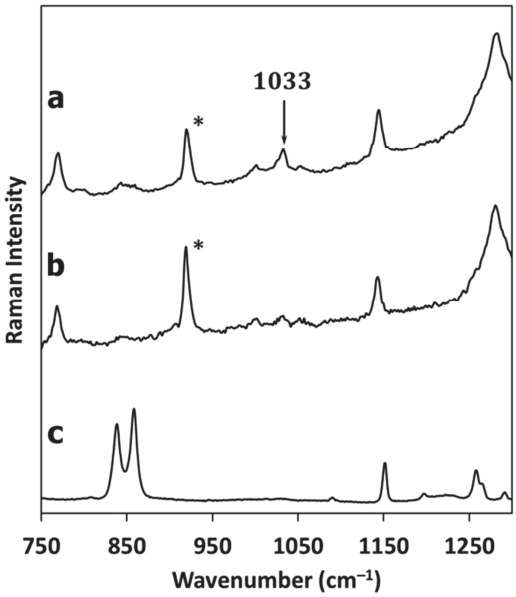

Figure 6.8: Raman spectra of (a) the yellow solution obtained after reaction of $[Cu^{II}(\mathbf{L^1SCH_3})](OTf)_2$ with $F\text{-}PhO^-$, (b) $[Cu^{II}(\mathbf{L^1SCH_3})(OPh\text{-}F)](OTf)$ and (c) F-PhOH recorded with a confocal Raman microscope at an excitation wavelength of 532 nm with 3 s exposure time; the spectra are the average of 25 accumulations. * = CH_3CN.

The formation of a Cu^I species, as confirmed by NMR and UV-vis spectroscopy, together with the appearance of a Raman band at 1033 cm^{-1} suggest the formation of a $PhO^{\bullet}$ radical that further reacts to form either a diaryl peroxide or an aromatic ether via a reaction with the solvent or the ligand. Further research will be directed toward isolation and characterization of this product. It is interesting to note that this reaction of $R\text{-}O^-$ to $R\text{-}O^{\bullet}$ is reminiscent of the Cu^{II} μ-thiolate/Cu^I disulfide redox chemistry (Chapter 1-3), in which $R\text{-}S^-$ is converted to R-S-S-R (Figure 6.9). This type of phenol redox chemistry is unprecedented and might explain the results of similar chemistry,

like for instance for the purple Cu^{II}-N(Sc)-Ts species that was reported to degrade to a Cu^{I} complex in aprotic solvents.[38]

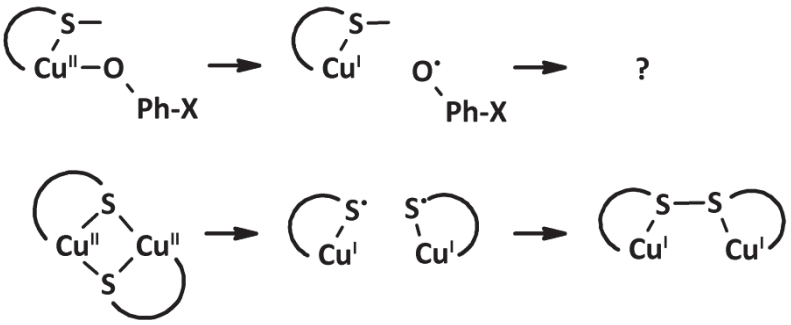

Figure 6.9: Schematic representation of the Cu^{II} μ-thiolate/Cu^{I} disulfide redox chemistry and the related Cu^{II} phenolate conversion to form Cu^{I} and a phenolate radical.

6.3 Conclusion

The unique find of the oxidation of substituted phenolates by Cu^{II} compounds to the corresponding phenolate radicals is described. Oxidation of a mixture of the Cu^{I} compound $[Cu^{I}(\mathbf{L^{1}SCH_{3}})]^{+}$ and phenol by air, results in the formation of a purple Cu^{II} phenolate species of which the structure was determined by X-ray crystallography. Isolation of $[Cu^{II}(\mathbf{L^{1}SCH_{3}}*)(OPh\text{-}Me)](PF_{6})$ indicated that this product degrades by reaction of the ligand at the benzylic positions of the pyridyl groups. The purple product converts to a yellow solution containing Cu^{I}, corroborated by NMR and UV-vis spectroscopy, and either a diaryl peroxide or an aromatic ether, as indicated by the appearance of a new Raman band. This reaction depends on the concentration of the mononuclear species and the *para*-substituent of the phenyl group; electron-donating substituents stabilize the purple Cu^{II} complex whereas electron-withdrawing substituents direct the conversion towards the diaryl peroxide. Interestingly, this reaction is very similar to the Cu^{II} μ-thiolate/Cu^{I} disulfide redox equilibrium. Such a redox reaction with Cu^{II} and phenolate has not been reported before to the best of our knowledge. Future research will be directed to further analysis and characterization of the product that is formed by the phenolate radical.

6.4 Experimental Section

6.4.1 General Methods

Reagents and solvents were purchased from commercial sources. Oxygen-free experiments were carried out using standard Schlenk-line techniques under an argon atmosphere.

$[Cu^{I}(CH_3CN)_4](PF_6)$ and $[Cu^{I}(CH_3CN)_4](SbF_6)$ were synthesized according to a literature procedure.[39] Potassium phenolate salts were obtained by adding potassium *tert*-butoxide to the corresponding phenol in tetrahydrofuran. NMR spectra were recorded on a Bruker 300 DPX spectrometer. NMR experiments under argon were carried out using a J. Young NMR tube. IR spectra were obtained on a Perkin Elmer UATR (Single Reflection Diamond) Spectrum Two device (4000-700 cm^{-1}; resolution 4 cm^{-1}). Mass spectrometry was performed using a Finnigan Aqua Mass Spectrometer (MS) with electro spray ionization (ESI). Sample introduction was achieved through a Dionex ASI-100 automated sample injector with an eluent flow rate of 0.2 mL/min. Elemental analyses were performed by the Microanalytical laboratory Kolbe in Germany. UV-vis spectra were collected using a transmission dipprobe with variable path length on an Avantes Avaspec-2048 spectrometer with Avalight-DH-S-BAL light source. Confocal Raman spectra at 532 nm were recorded using a Renishaw InVia Reflex Raman microscope (Wotton-under-Edge, United Kingdom) with a 300 mW, 785 nm diode laser in combination with a 1200 lines per millimeter (l/mm) grating and an 80 mW, 532 nm frequency doubled Nd:YAG excitation source in combination with a 1800 l/mm grating and a Peltier cooled CCD detector (203 K). The instrument included a Leica light microscope 5× and 20× air objectives. The 521 cm^{-1} Raman shift of an internal silicon standard was used to verify the calibration of the system. Cyclic voltammetry was performed with an Autolab PGstat10 potentiostat controlled by GPES4 software. A three-electrode arrangement with a glassy carbon working electrode (3 mm diameter), an Ag/AgCl double junction reference electrode and a Pt wire counter electrode were used in different solvents with 0.1 M NBu_4PF_6 as the electrolyte. In these conditions the Fc/Fc^+ couple was found to be located at +443 mV with a peak-to-peak separation of 60 mV in CH_3CN. Potentials are given relative to the Ag/AgCl electrode.

6.4.2 X-ray Crystallography

The reflection intensities for $[Cu^{II}(\mathbf{L^1SCH_3})(Cl)](BF_4)$, $[Cu^{II}(\mathbf{L^1SCH_3})(OPh)](SbF_6)$ and $[Cu^{II}(\mathbf{L^1SCH_3}^*)(OPh\text{-}Me)](PF_6)$ were collected at 110(2) K using a SuperNova diffractometer (equipped with Atlas detector) with Mo $K\alpha$ radiation (λ = 0.71073 Å) for $[Cu^{II}(\mathbf{L^1SCH_3})(Cl)](BF_4)$ and Cu Kα radiation (λ = 1.54178 Å) for $[Cu^{II}(\mathbf{L^1SCH_3})(OPh)](SbF_6)$ and $[Cu^{II}(\mathbf{L^1SCH_3}^*)(OPh\text{-}Me)](PF_6)$ under the program CrysAlisPro (Version 1.171.36.32 Agilent Technologies, 2013). The program was used to refine the cell dimensions and for data reduction. The structure was solved with the program SHELXS-2013 or SHELXS-2014 (Sheldrick, 2013-2014)[40] and was refined on F^2 with SHELXL-2013 or SHELXL-2014 (Sheldrick, 2013-2014).[40] Analytical numeric absorption corrections based on a multifaceted crystal model were applied using CrysAlisPro. The temperature of the data collection was controlled using the system Cryojet (manufactured by Oxford Instruments). The H atoms were placed at calculated positions using the instructions AFIX 13, AFIX 23, AFIX 43, AFIX 137 or AFIX 147 with isotropic displacement parameters having values 1.2 or 1.5 times *U*eq of the attached C or O(O2/O2') atoms. The crystals of $[Cu^{II}(\mathbf{L^1SCH_3})(OPh)](SbF_6)$ were found to be pseudo-merohedrally twinned. The twin relationship is defined by the matrix: (1 0 0 / 0 –1 0 / 0 0 –1).

The BASF factor refines to 0.1550(10). The H atom attached to O3 (from the non-coordinated *p*-cresol in [Cu^{II}(**L^1SCH_3***)(OPh-Me)](PF_6)) was found from difference Fourier map, and its coordinates and isotropic temperature factor were refined freely.

6.4.3 Ligand and Complex Synthesis

L^1SCH_3

The synthesis of **L^1SCH_3** was carried out using a slightly modified literature procedure.[41] 2-Pyridinecarboxaldehyde (1.90 mL, 20 mmol) was added to 2-(methylthio)ethylamine (0.93 mL, 10 mmol) dissolved in dichloromethane (20 mL). $NaBH(OAc)_3$ (6.0 g, 28 mmol) was added in small portions over the course of 30 min and the solution was stirred for approximately 5 hours at RT. The reaction was quenched by slowly adding 50 mL NaOH (2 M). The two layers were separated and water layer was washed two more times with dichloromethane. The combined organic layers were dried over Na_2SO_4 after which the solution was evaporated to dryness yielding an orange/yellow oil (2.7 g, 9.9 mmol, 99%). ^{1}H NMR (300 MHz, CD_3CN, RT): δ 1.97 (s, 3H, S-C*H*$_3$), 2.64 (m, 2H, S-C*H*$_2$-C*H*$_2$), 2.74 (m, 2H, S-C*H*$_2$-C*H*$_2$), 3.80 (s, 4H, Py-C*H*$_2$-N), 7.18 (m, 2H, Py-*H*$_5$), 7.56 (d, *J* = 8 Hz, 2H, Py-*H*$_3$), 7.70 (td, *J* = 8 Hz, 2 Hz, 2H, Py-*H*$_4$), 8.47 (m, 2H, Py-*H*$_6$). ^{13}C NMR (75 MHz, CD_3CN, RT): δ 15.6 (S-CH_3), 32.3 (S-CH_2-CH_2), 54.2 (S-CH_2-CH_2), 60.8 (Py-CH_2-N), 122.9 (Py-*C*$_3$ or Py-*C*$_5$), 123.8 (Py-*C*$_3$/Py-*C*$_5$), 137.3 (Py-*C*$_4$), 149.8 (Py-*C*$_6$), 160.7 (Py-*C*$_2$). ESI-MS found (calculated) for $[M+H]^+$ *m*/*z* 274.1 (274.1). IR (neat, cm^{-1}): 2915*w*, 2829*w*, 1589*s*, 1569*m*, 1473*m*, 1432*s*, 1362*m*, 1117*m*, 1047*m*, 994*m*, 755*s*, 616*m*.

*[Cu^{II}(**L^1SCH_3**)(Cl)](BF_4)*

To a solution of **L^1SCH_3** (94 mg, 0.34 mmol) in 8 mL MeOH, [$Cu^{II}(H_2O)_6$](BF_4)$_2$ (59 mg, 0.17 mmol) and $CuCl_2 \cdot 2\ H_2O$ (29 mg, 0.17 mmol) were added, after which a precipitate formed. The precipitate was filtered and washed with MeOH and Et_2O, which yielded the product as a dark blue crystalline solid (110 mg, 0.24 mmol, 70%). Crystals suitable for X-ray structure determination were obtained by slow vapor diffusion of diethyl ether into a methanol solution containing the complex. Elemental analysis calcd for [Cu^{II}(**L^1SCH_3**)(Cl)](BF_4), $C_{15}H_{19}BClCuF_4N_3S$: C 39.23, H 4.17, N 9.15, S 6.98; Found: C 39.73, H 4.44, N 9.25, S 7.05. ESI-MS found (calculated) for $[M - BF_4]^+$ *m*/*z* 370.9 (371.0). IR (neat, cm^{-1}): 1611*m*, 1441*m*, 1284*m*, 1046*vs*, 1029*vs*, 1002*m*, 907*m*, 783*m*, 759*m*, 519*m*. UV-vis in acetonitrile at 0.1 mM [Cu] concentration: 258 nm (ε = 10 800 M^{-1} cm^{-1}), 297 nm (ε = 3 400 M^{-1} cm^{-1}), 700 nm (ε = 130 M^{-1} cm^{-1}), 890 nm (ε = 170 M^{-1} cm^{-1}).

*[Cu^{II}(**L^1SCH_3**)(OPh)](SbF_6)*

L^1SCH_3 (70.5 mg, 0.26 mmol) was dissolved in 35 mL CH_2Cl_2 under argon atmosphere using standard Schlenk-line techniques. To this yellow solution [$Cu^{I}(CH_3CN)_4$](SbF_6) (120 mg, 0.26 mmol) and phenol (25.0 mg, 0.26 mmol) were added. The solution was opened to air and changed color from brown/yellow to intense dark purple. After 15 minutes stirring in air, 70 mL of *n*-pentane was added, which resulted in the formation of a precipitate that was collected

by filtration and was washed with *n*-pentane to yield [Cu^{II}(**L^1SCH_3**)(OPh)](SbF_6) as a dark brown powder (135 mg, 0.20 mmol, 79%). Crystals suitable for X-ray structure determination were obtained by storing a CH_2Cl_2 solution of the complex in an NMR tube in the freezer at –84 °C. Elemental analysis calcd for [Cu^{II}(**L^1SCH_3**)(OPh)](SbF_6), $C_{21}H_{24}CuF_6N_3OSSb$: C 37.88, H 3.63, N 6.31, S 4.82. Found: C 37.69, H 3.74, N 6.29, S 4.79. ESI-MS found (calculated) for [M – OPh – SbF_6]$^+$ *m*/*z* 336.0 (336.1); [M + Cl – OPh – SbF_6]$^+$ *m*/*z* 371.0 (371.0). IR (neat, cm^{-1}): 1609*m*, 1585*w*, 1475*m*, 1447*w*, 1284*w*, 1264*m*, 1239*m*, 1160*w*, 1032*w*, 819*w*, 763*s*, 696*w*, 653*vs*, 574*w*, 541*w*, 515*w*. UV-vis in acetonitrile at 1.0 mM [Cu] concentration: 238 nm (ε = 9 300 M^{-1} cm^{-1}), 255 nm (ε = 8 800 M^{-1} cm^{-1}), 293 nm (ε = 3 700 M^{-1} cm^{-1}), 320 nm (ε = 3 000 M^{-1} cm^{-1}), 510 nm (ε = 700 M^{-1} cm^{-1}) and 840 nm (ε = 380 M^{-1} cm^{-1}).

*[Cu^{II}(**L^1SCH_3***)(OPh-Me)](PF_6)*

Crystals of [Cu^{II}(**L^1SCH_3***)(OPh-Me)](PF_6) were obtained in a similar way as [Cu^{II}(**L^1SCH_3**)(OPh)](SbF_6), but starting from *p*-cresol and [Cu^{I}(CH_3CN)$_4$](PF_6). Crystals suitable for X-ray structure determination were obtained by vapor diffusion at –20 °C of *n*-pentane into a CH_2Cl_2 solution containing the complex mixture.

6.5 References

1. Lewis, E. A.; Tolman, W. B., *Chem. Rev.* **2004,** *104*, 1047-1076.
2. Solomon, E. I.; Heppner, D. E.; Johnston, E. M.; Ginsbach, J. W.; Cirera, J.; Qayyum, M.; Kieber-Emmons, M. T.; Kjaergaard, C. H.; Hadt, R. G.; Tian, L., *Chem. Rev.* **2014,** *114*, 3659-3853.
3. Koval, I. A.; Gamez, P.; Belle, C.; Selmeczi, K.; Reedijk, J., *Chem. Soc. Rev.* **2006,** *35*, 814-840.
4. Sánchez-Ferrer, A.; Rodríguez-López, J. N.; García-Cánovas, F.; García-Carmona, F., *Biochim. Biophys. Acta* **1995,** *1247*, 1-11.
5. Yamazaki, S.; Itoh, S., *J. Am. Chem. Soc.* **2003,** *125*, 13034-13035.
6. Fujieda, N.; Murata, M.; Yabuta, S.; Ikeda, T.; Shimokawa, C.; Nakamura, Y.; Hata, Y.; Itoh, S., *J. Biol. Inorg. Chem.* **2013,** *18*, 19-26.
7. Allen, S. E.; Walvoord, R. R.; Padilla-Salinas, R.; Kozlowski, M. C., *Chem. Rev.* **2013,** *113*, 6234-6458.
8. Osako, T.; Ueno, Y.; Tachi, Y.; Itoh, S., *Inorg. Chem.* **2004,** *43*, 6516-6518.
9. Ambundo, E. A.; Deydier, M. V.; Grall, A. J.; Aguera-Vega, N.; Dressel, L. T.; Cooper, T. H.; Heeg, M. J.; Ochrymowycz, L. A.; Rorabacher, D. B., *Inorg. Chem.* **1999,** *38*, 4233-4242.
10. Mirica, L. M.; Ottenwaelder, X.; Stack, T. D. P., *Chem. Rev.* **2004,** *104*, 1013-1045.
11. Socrates, G., *Infrared and Raman Characteristic Group Frequencies: Tables and Charts*. 3rd ed.; Wiley: **2004**.
12. Donoghue, P. J.; Tehranchi, J.; Cramer, C. J.; Sarangi, R.; Solomon, E. I.; Tolman, W. B., *J. Am. Chem. Soc.* **2011,** *133*, 17602-17605.

13. King, A. E.; Huffman, L. M.; Casitas, A.; Costas, M.; Ribas, X.; Stahl, S. S., *J. Am. Chem. Soc.* **2010,** *132*, 12068-12073.
14. McDonald, M. R.; Scheper, W. M.; Lee, H. D.; Margerum, D. W., *Inorg. Chem.* **1995,** *34*, 229-237.
15. McDonald, M. R.; Fredericks, F. C.; Margerum, D. W., *Inorg. Chem.* **1997,** *36*, 3119-3124.
16. While running checkCIF, the checking procedure generated the following alert type A: *"Structure contains solvent accessible voids of 416 Å^3"*. The highest residual electron density peak and hole are 1.01 (located at 0.94 Å from Sb1) and –0.86 e$^-$ Å^{-3} (located at 0.80 Å from Sb1), respectively. The second largest peak (0.84 e$^-$ Å^{-3}) and two other peaks (0.64 and 0.43 e$^-$ Å^{-3}) that are found in those voids are most likely concerned with some residual disordered solvent molecules with very low occupancy factors. Thus, this alert can be disregarded as there is no significant effect on the correctness of the structure.
17. Addison, A. W.; Rao, T. N.; Reedijk, J.; Vanrijn, J.; Verschoor, G. C., *J. Chem. Soc., Dalton Trans.* **1984**, 1349-1356.
18. One CH_2Cl_2 molecule is found to be disordered over two orientations. The occupancy factors of both major and minor components refine to 0.726(5) and 0.211(5). The other CH_2Cl_2 molecule is ordered, but its occupancy factor refines to 0.809(4).
19. Arnold, P. J.; Davies, S. C.; Dilworth, J. R.; Durrant, M. C.; Griffiths, D. V.; Hughes, D. L.; Richards, R. L.; Sharpe, P. C., *J. Chem. Soc., Dalton Trans.* **2001**, 736-746.
20. Letko, C. S.; Rauchfuss, T. B.; Zhou, X.; Gray, D. L., *Inorg. Chem.* **2012,** *51*, 4511-4520.
21. van der Vlugt, J. I.; Pidko, E. A.; Vogt, D.; Lutz, M.; Spek, A. L., *Inorg. Chem.* **2009,** *48*, 7513-7515.
22. Filonenko, G. A.; Cosimi, E.; Lefort, L.; Conley, M. P.; Copéret, C.; Lutz, M.; Hensen, E. J. M.; Pidko, E. A., *ACS Catal.* **2014,** *4*, 2667-2671.
23. Vacque, V.; Sombret, B.; Huvenne, J. P.; Legrand, P.; Suc, S., *Spectrochim. Acta A* **1997,** *53*, 55-66.
24. Green, J. H. S.; Harrison, D. J.; Kynaston, W., *Spectrochim. Acta A* **1971,** *27*, 2199-2217.
25. Shamovsky, I. L.; Riopelle, R. J.; Ross, G. M., *J. Phys. Chem. A* **2001,** *105*, 1061-1070.
26. Asatryan, R.; Davtyan, A.; Khachatryan, L.; Dellinger, B., *J. Phys. Chem. A* **2005,** *109*, 11198-11205.
27. Drew, M. G. B.; Hopkins, W. A.; Mitchell, P. C. H., *J. Chem. Soc., Faraday Trans.* **1990,** *86*, 47-52.
28. Benassi, R.; Folli, U.; Sbardellati, S.; Taddei, F., *J. Comput. Chem.* **1993,** *14*, 379-391.
29. Li, H.-M.; Zhao, S.-R.; Huo, Q.; Ma, T.; Liu, H.; Lee, J.; Hong, Y.-S.; Wu, C.-Z., *Arch. Pharmacal Res.* **2014**, 1-6.
30. de Mesquita, M. L.; Araújo, R. M.; Bezerra, D. P.; Filho, R. B.; de Paula, J. E.; Silveira, E. R.; Pessoa, C.; de Moraes, M. O.; Costa Lotufo, L. V.; Espindola, L. S., *Biorg. Med. Chem.* **2011,** *19*, 623-630.

31. Palacios-Hernández, T.; Höpfl, H.; Sánchez-Salas, J. L.; González-Vergara, E.; Pérez-Benítez, A.; Quiroz-Alfaro, M. A.; Méndez-Rojas, M. A., *J. Inorg. Biochem.* **2014,** *139*, 85-92.
32. Bayrakçeken, F.; Aktaş, S.; Toptan, M.; Ünlügedik, A., *Spectrochim. Acta A* **2003,** *59*, 135-138.
33. Goyal, R. N.; Sangal, A., *J. Electroanal. Chem.* **2005,** *578*, 185-192.
34. Lin, Y.-W.; Sun, M.-H.; Wan, D.; Liao, L.-F., *Spectrochim. Acta A* **2012,** *96*, 365-369.
35. Tao, Z.; Li, Z., *Int. J. Chem. Kinet.* **1999,** *31*, 65-72.
36. Field, R. J.; Raghavan, N. V.; Brummer, J. G., *J. Phys. Chem.* **1982,** *86*, 2443-2449.
37. Colthup, N. B.; Daly, L. H.; Wiberley, S. E., *Introduction to Infrared and Raman Spectroscopy*. 3rd ed.; Academic Press: San Diego, **1990**.
38. Kundu, S.; Miceli, E.; Farquhar, E.; Pfaff, F. F.; Kuhlmann, U.; Hildebrandt, P.; Braun, B.; Greco, C.; Ray, K., *J. Am. Chem. Soc.* **2012,** *134*, 14710-14713.
39. Kubas, G. J., *Inorg. Synth.* **1990,** *28*, 68-70.
40. Sheldrick, G. M., *Acta Crystallogr. Sect. A* **2008,** *64*, 112-122.
41. Schatz, M.; Leibold, M.; Foxon, S. P.; Weitzer, M.; Heinemann, F. W.; Hampel, F.; Walter, O.; Schindler, S., *Dalton Trans.* **2003**, 1480-1487.